Vietnam Journal of Earth Sciences, 44(1), 73-91, https://doi.org/10.15625/2615-9783/16874

Vietnam Academy of Science and Technology
Vietnam Journal of Earth Sciences
http://www.vjs.ac.vn/index.php/jse

Sea surface temperature trend analysis by Mann-Kendall test and sen's slope estimator: a study of the Hai Phong coastal area (Vietnam) for the period 1995-2020

Vu Duy Vinh*[1], Sylvain Ouillon[2,3], Nguyen Minh Hai[1,4]

[1]*Institute of Marine Environment and Resources, VAST, Haiphong City 04216, Vietnam*
[2]*UMR LEGOS, University of Toulouse, IRD, CNES, CNRS, UPS, 14 avenue Edouard Belin, 31400 Toulouse, France*
[3]*Department Water-Environment-Oceanography, University of Science and Technology of Hanoi (USTH), VAST, Hanoi 100000, Vietnam*
[4]*Graduate University of Science and Technology, VAST, Hanoi, Vietnam*

Received 07 October 2021; Received in revised form 11 December 2021; Accepted 10 January 2022

ABSTRACT

Based on the Mann-Kendall test and Sen's slope method, this study investigates the monthly, seasonal, and annual sea surface temperature (SST) trends in the coastal area of Hai Phong (West of Tonkin Gulf) based on the measurements at Hon Dau Station from 1995 to 2020. The results show a sea surface warming trend of 0.02°C/year for the period 1995-2020 (significant level $\alpha = 0.1$) and of 0.093°C/year for the period 2008-2020 (significant level $\alpha = 0.05$). The monthly SSTs in June and September increased by 0.027°C/year and 0.036°C/year, respectively, for the period 1995-2020, and by 0.080°C/year and 0.047°C/year, respectively, for the period 2008-2020. SST trends in winter, summer, and other months were either different for the two periods or not significant enough. This may be due to the impact of ENSO, which caused interannual SST variability in the Hai Phong coastal with two intrinsic mode functions (IMF) signals a period of ~2 (IMF3) and ~5.2 years cycle (IMF4). A combination of these signals had a maximum correlation of 0.22 with ONI (Oceanic Niño Index) delayed by 8 months. ENSO events took ~8 months to affect SST at Hai Phong coastal area for 1995-2020 and caused a variation of SST within 1.2°C.

Keywords: sea surface temperature, warming, trend, Mann-Kendall, Sen slope, ENSO, Hai Phong.

1. Introduction

Climate change is seen to be affecting the whole world, and there has been and still is a growing concern about its trend and consequences. However, understanding of climate change effects in the coastal area is limited. It is a challenge for spatial planning, management, and conservation strategies to develop solutions for adaptation to climate change (Groves et al., 2012; Watson et al., 2012). Recent studies (Yu et al., 2019; NOAA, 2021) have shown that the manifestations of climate change are markedly higher in these areas than anywhere else in the world, including a rapid increase in

*Corresponding author, Email: vinhvd@imer.vast.vn

sea surface temperatures (SST). According to NOAA (2021), the decadal global land and ocean surface, average temperature anomaly for 2011-2020 was the warmest decade on record for the globe, with a global surface temperature of +0.82°C above the 20th-century average, and surpassed the previous decadal record (2001-2010) value of +0.62°C.

Water temperature is one of the essential control factors for water quality and marine ecosystem health (O'Connor et al., 2007; Scholes et al., 2014). It influences several other parameters and some physical and chemical properties of water. For example, the water temperature can affect aquatic organisms' metabolic rates and biological activity (Wetzel, 2001). It influences the habitats chosen by marine species (EPA, 2012). Some aquatic plants thrive in warmer temperatures, while some fish species such as trout or salmon prefer colder streams (EPA, 2012). Increased respiration rates at higher temperatures lead to increased oxygen consumption, which can be detrimental if rates remain high for an extended period. Temperature can also inhibit plant respiration and photosynthesis. In general, algal photosynthesis increases with temperature, although different species have different maximum temperatures for optimal photosynthetic activity (Wetzel, 2001). Therefore, the study of rising sea temperatures is essential to assess the effects of climate change on marine resources and the environment.

SST is influenced by air temperature and factors such as solar radiation, its degree of blockage by obstacles, the water temperature of the rivers draining the catchments areas, and heat exchange at the water surface. Therefore, the variation of SST is more complex than the air temperature and has a higher spatial variation (Pasquero, 2008).

Recently studies have shown that Asia had its warmest year on record in 2020, with a temperature difference of 2.07°C above the 1910-2000 average, for the first time exceeding 2.0°C in annual data. Asia's ten warmest years have occurred since 2002, while the five warmest years have all occurred since 2007 (NOAA, 2021). This is also the 33rd consecutive year that Asia has experienced above-average temperatures. During the 1910-2020 period, Asia's trend was 0.17°C per decade, and the 1981-2020 trend (0.37°C per decade) was twice as high as this longer-term trend (NOAA, 2021). Yu et al. (2019) reported that from 2003 to 2017, the average water temperature in the East Sea increased by about 0.031°C/year with the most robust warming identified in southeastern Vietnam.

Several approaches are available for the assessment of the trends. Among them, the Mann-Kendall (MK) trend test (Mann, 1945; Kendall, 1975), the Sen's slope estimator (Sen, 1968), and the Şen's Iterative trend analysis (Şen, 2012) are most widely used for hydrological trend analysis (Zakwan and Ahmad, 2021; Ali et al., 2019; Güçlü, 2018, Tosunoglu and Kisi, 2017), water quality (Hirsch et al., 1982; Hirsch and Slack, 1984; Burn et al., 2012), temperature and precipitation (Sang et al., 2014; Wang S. et al., 2019), and sea-level rise (Wahl et al., 2011; Chandler and Scott, 2011; Ca, 2017; Ozgenc Aksoy, 2017). The MK test is usually used to detect an increasing or decreasing trend in a series of hydrological, climatic, or environmental data. The null hypothesis for this test indicates no trend, whereas the alternative view suggests a direction in a two- or one-sided test as an increasing trend or decrease trend (Pohlert, 2020). Sen’s estimator is another non-parametric method to identify the trend magnitude. This method computes the linear rate of the slope and the intercept, as shown in Sen’s approach (Sen, 1968). The combining of MK test and Sen’s pitch is widely documented in various literature, as a

powerful trend test for practical analysis of seasonal and annual trends, and is preferred over other tests because of its applicability to data time series that do not follow a statistical distribution (Duan et al., 2019; Gao et al., 2019; Dong et al., 2019, Alemu and Dioha, 2020). Thus, this study has employed the MK trend test and Sen's slope estimate to understand the SST trend and significance level in the Hai Phong coastal area.

With a long coastline and a large continental shelf area, Vietnam is expected to suffer many negative impacts of climate change (ADB, 2013). Therefore, there have been many studies on the effects of climate change on the Vietnam coastal areas. However, the variation of seawater temperature in the East Saunder impacts climate change is not well documented. There have been a few studies on the trend of SST, but their results and variations (monthly, seasonal) over time have not been analyzed in detail (MONRE, 2016; Ca, 2017; Chung and Long, 2016). In addition, the published articles are limited to data collected until 2014. This paper aims to investigate the trend of SST in the Hai Phong coastal area at Hon Dau Station (Fig. 1) in recent years (1995-2020 and 2008-2020) based on the MK test and Sen's slope. The trends of SST and their descriptive statistics from this study will help better understand the impact of climate change on the marine environment in the northeast region of Vietnam's Sea.

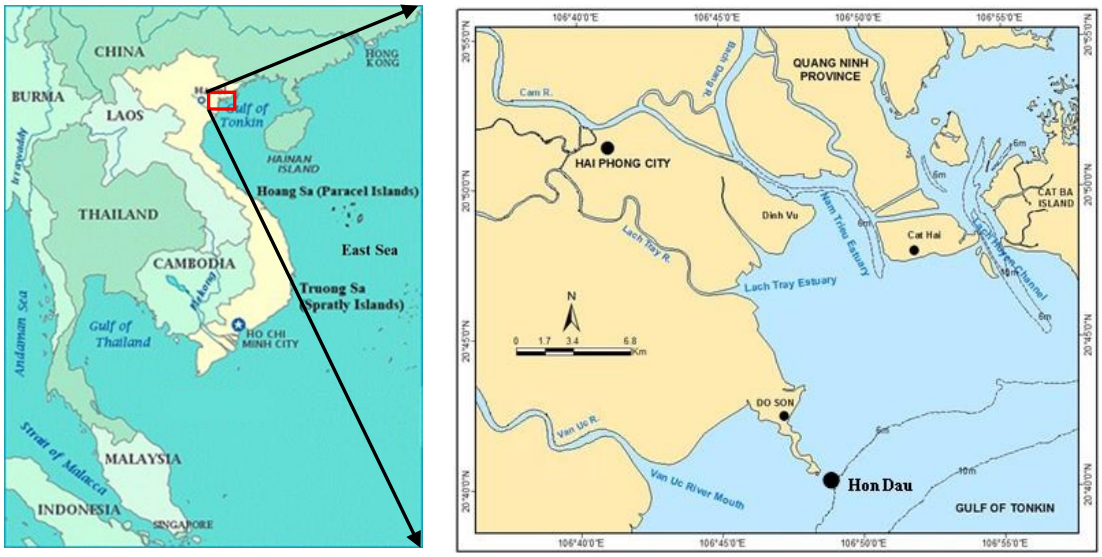

Figure 1. Hon Dau station in Hai Phong coastal area

2. Material and methods

2.1. Hai Phong coastal area

Hai Phong's coastal area is located in the northeastern maritime region of Vietnam (western of Tonkin Gulf), 120 km away from Hanoi (Fig. 1). Hai Phong is the third-largest city in Vietnam and has the largest seaport in the northern region (Vinh & Ouillon, 2021). With a long coastline of 125 km, including the islands off the coast, the sea covers an area of about 4000 square kilometers; Hai Phong coastal areas have great potential for marine resources. There are nearly 1,000 species of shrimp, fish including dragon shrimps, prawns, crabs, tortoises, oysters, dolphins, pearls, abalone, etc., and dozens of species of seaweeds with high economic values (Thanh et al., 2015).

A tropical monsoon climate influences this area with a dry winter and a wet summer.

Based on measurements at Hon Dau Station from 1978 to 2007, the annual rainfall in the region was 1161 mm, which is mainly concentrated in summer with 83% of annual rainfall between May and October (Duy Vinh et al., 2018). Analysis of wind data at Hon Dau (1960-2011) showed that the dominant winds are from the East (NE, E, SE) and South (SW, S, SE) directions at 72.2% in the wet season (June to September), and from the North (NE, N, NW) and East (SE, E, NE) directions at 92.1% during the dry season (December to March).

Hai Phong coastal area is strongly affected by the hydrological regime of the Red River (Vinh and Uu, 2013; Lefebvre et al., 2012; Vinh and Thanh, 2014). Based on data from 1960 to 2010, the Red River discharge at Son Tay (near the apex of the Red River delta) has varied over the range 80.5 (2010)-160.7 (1971) × 10^9 m^3 $year^{-1}$, with an average value of 110.0 × 109 m^3 $year^{-1}$. The river discharge experiences substantial seasonal variations, with 71-79% of annual total water discharge in the rainy season and only 9.4-18% during the dry season (Vinh et al., 2014). The Cam-Nam Trieu estuary is affected mainly by diurnal tides (Minh et al., 2014). According to the tide gauge measurements at Hon Dau station (1960-2011), the tidal range is about 2.6-3.6 m in spring tide and about 0.5-1.0 m in the neap wave.

2.2. Data

The SST measured data at Hon Dau Station is used in this study. The Hon Dau station is a national marine hydrometeorological station in the coastal area of Hai Phong, located at position 20°40'N-106°48'E (Fig. 1), and established in 1958. These data are measured in situ four times per day (at 1h, 7h, 13h, and 19h) by the National Hydro-Meteorological Service. The SST has been measured since 1958 but, due to the long war and lack of funds for high-quality equipment, the data was not of good quality in the period before the "Doi moi" and was not available at certain times. Especially in the period from 1970 to 1994, there were many months without data. Furthermore, as rising temperatures may be increasing in recent years, we decided to restrict this study to good quality data acquired since 1995 to extract trends over the whole period 1995-2020 and the shortest and more recent period 2008-2020.

In addition, monthly mean Oceanic Niño Index (ONI) data for the period 1995-2020 were extracted from the NOAA Center for Weather and Climate Prediction database (http://www.cpc.ncep.noaa.gov). The ONI is used to identify El Niño (warm) and La Niña (cold) events in the Tropical Pacific. The ONI is based on the 3-month moving average of the SST anomaly in the Nino 3.4 region (5°N -5°S, 120°W-170°W). An El Niño event is considered when the ONI exceeds the threshold value +0.5°C for at least 5 consecutive months. Conversely, La Niña events are defined as periods with at least five consecutive months with an ONI below -0.5°C (NOAA, 2020)

2.3. Methodology of trend analysis

2.3.1. The Mann-Kendall test

The Mann-Kendall test is a widely used statistical test to identify the existence of trends in climatological and hydrological time series. In this test, the null hypothesis H_0 assumes that there is no trend (the data is independent and randomly ordered), tested against the alternative hypothesis H_1, which assumes a trend. X_i and X_j are two subsets of data where i = 1, 2, 3,…, n − 1 and j = i + 1, i + 2, i + 3,…, n.

The Mann-Kendall statistic parameter - S is computed as follows:

$$S = \sum_{i=1}^{n-1} \sum_{j=i+1}^{n} sign(X_j - X_i) \quad (1)$$

$$Sign\left(X_j - X_i\right) = \begin{cases} 1 \; if \; X_j - X_i > 0 \\ 0 \; if \; X_j - X_i = 0 \\ -1 \; if \; X_j - X_i < 0 \end{cases} \quad (2)$$

The variance of S, VAR (S) is given by

$$VAR(S) = \frac{n(n-1)(2n+5)-\sum_{p=1}^{m} t_p(t_p-1)(2t_p+5)}{18} \quad (3)$$

where n is the number of data points, m is the number of unique values (without duplicates), and t_p is the number of data values in the p^{th} group.

The standard test statistic Z_s is calculated as follows:

$$Z_S = \begin{cases} \frac{S-1}{\sqrt{VAR(S)}} & \text{for } S > 0 \\ 0 & \text{for } S = 0 \\ \frac{S+1}{\sqrt{VAR(S)}} & \text{for } S < 0 \end{cases} \quad (4)$$

A positive (negative) value of Z_s indicates an upward (downward) trend. The value of statistic Z_s is the MK test statistic that follows a standard normal distribution with mean 0 and variance 1. To test for either an upward or downward monotone trend (a two-tailed test) at α level of significance, H_0 is rejected if the absolute value of Z_s is greater than $Z_{1-\alpha/2}$, where $Z_{1-\alpha/2}$ is obtained from the standard normal cumulative distribution tables. If $|Z_s|$ is greater than $Z_{\alpha/2}$, where α represents the chosen significance level (α =10% at the 90% confidence level with $Z_{0.05}$ = 1.65; α =5% at the 95% confidence level with $Z_{0.025}$ = 1.96; α =1% at the 99% confidence level with $Z_{0.005}$ = 2.58), then the null hypothesis is invalid implying that the trend is significant.

The Z_s value can be related to a P-value of a specific trend. The P-value corresponds to the probability of observing sample data at least as extreme as the obtained test statistic. Small *p*-values provide evidence against the null hypothesis. The smaller (closer to 0) the P-value, the stronger is the evidence against the null hypothesis. If the P-value is less than or equal to the specified significance level *α*, the null hypothesis is rejected; otherwise, the null hypothesis is not rejected. In other words, if P ≤ *α*, reject H_0; otherwise, if P > *α,* do not reject H_0 (Davis, 2002).

2.3.2. Sen's slope estimator

Sen (1968) proposed the non-parametric procedure for estimating the slope of trend in the sample of N pairs of data:

$$Q_i = \frac{X_j - X_k}{j-k} \quad (5)$$

where i=1, ..., N. x_j and x_k are the data values at time j and k (j > k), respectively.

If there is only one datum in each time period, then $N = \frac{n(n-1)}{2}$, where n is the number of time periods. Otherwise, if there are multiple observations in one or more time periods, then $N < \frac{n(n-1)}{2}$, where n is the total number of observations.

The N values of Q_i are ranked from smallest to largest and the median of slope or Sen's slope, and can be calculated as follows:

$$Q_{med} = \begin{cases} Q_{\left[\frac{N+1}{2}\right]} & \text{if N is odd} \\ \frac{Q_{N/2}+Q_{(N+2)/2}}{2} & \text{if N is even} \end{cases} \quad (6)$$

The Q_{med} sign reflects data trend, while its value indicates the steepness of the trend.

3. Results

3.1. Temporal variation of water temperature in Hai Phong coastal area

Located in the region affected by the tropical monsoon climate regime, the water temperature in the Hai Phong coastal area varies seasonally. Monthly averages calculated over 1995-2020 show that SST increases gradually from January to March and rapidly from March to May, peaks in June-July (at 30.2°C on average), then decrease steadily to January. The mean monthly SST remains above 28°C from May (28.5°C) to September (29.7°C). In contrast, SST remains in average below 22°C from December (21.1°C) to March (21.0°C), with the lowest value in January (19.3°C) (Fig. 2, Table 1). To assess the seasonal fluctuations of the SST, we took the months with average temperatures greater than 29.66°C as summer months and smaller than 19.32°C as winter months. The temperature

difference between the winter (December to March) and summer months (June to September) was above 10°C.

Maximum monthly SST ranged from 31.49°C in July and 21.35°C in January. From June to September, these maximum values exceed 30°C. During the winter months, they never exceed 23.5°C (Fig. 2, Table 1).

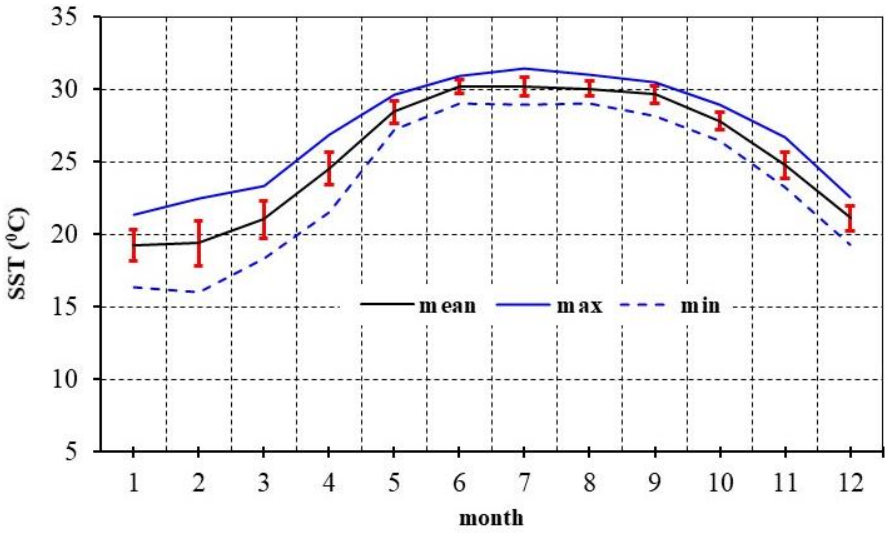

Figure 2. Monthly water SST (mean, max, min), and standard deviation (Red column) for the period 1995-2020 in Hon Dau Station

Table 1. Statistical information on SST (°C) for the period 1995-2020 in Hon Dau Station

Month\year	Maximum	Minimum	Mean	Std Dev	CV(%)
1	21.35	16.39	19.27	1.10	5.69
2	22.51	16.01	19.39	1.56	8.02
3	23.34	18.35	21.03	1.30	6.19
4	26.91	21.57	24.56	1.13	4.60
5	29.67	27.23	28.46	0.76	2.67
6	30.98	29.01	30.21	0.43	1.43
7	31.49	28.95	30.21	0.62	2.04
8	30.99	29.01	30.08	0.51	1.70
9	30.50	28.21	29.66	0.58	1.96
10	28.96	26.43	27.83	0.62	2.23
11	26.69	23.25	24.81	0.92	3.69
12	22.59	19.32	21.12	0.86	4.08
Year	**26.60**	**24.63**	**25.55**	**0.43**	**1.69**

The calculated standard deviation (Std Dev) also shows that the summer SST is close to the mean, with an Std Dev less than 1°C and a coefficient of variation (CV) of about 2% in the mid-summer (Table 1). The higher Std Dev in winter (from 0.9 to 1.6°C, with a CV ranging from 4.1 to 8%) show that the mean SST varies over a wider range in this season.

Monthly minimum SST averages ranged from 16°C in February to 29.1°C in June and August. In winter, these monthly minima did not exceed 19.32°C, while in the summer, they were no lower than 27.3°C (Fig. 2, Table 1).

3.2. Trends of SST for the period 1995-2020

The mean annual SST at Hon Dau station over 1995-2020 varies significantly from year to year, around a 26-year average of 25.55°C. The yearly maximum of SST reached 26.6°C in 2019, 1.1°C above the interannual average, while the minimum of 24.63°C, 0.9°C below the average, was acquired in 2011 (Table 1, Fig. 3a). The calculations show that the mean annual SST is close to the interannual mean with a standard deviation of about 0.4°C and CV values below 2% (Table 1).

The time series of annual SST at Hon Dau station shows an apparent increase (Fig. 3a). The linear regression equation for annual SST shows a positive slope value (a = 0.0221) for a

coefficient of determination R^2 of 0.1536. Therefore, 15% of the variability in the annual SST is explained by this linear regression model.

The trend of SST for Hon Dau station was analyzed by the Mann-Kendall test and Sen's slope estimator. The positive Kendall's S value (77) indicates an upward trend of SST over time. The Z parameter (1.68), greater than 1.65, confirms a significant trend. The P-value =0.094 is below the considerable level α = 0.1 (Table 2), leading to a trend at the 90% confidence level. Sen's slope for the annual mean SSTs indicates an increasing trend of 0.02°C/year at Hon Dau over 1995-2020 (Table 2).

Table 2. Trend analysis of annual mean SST using the Mann-Kendall test and Sen's slope for period 1995-2020

Periods/time	P-value	MK (Z)	MK Test (S)	Significance level (α)	Slope (°C/year)	Trend
1	0.724340	-0.35	-17	0.1	-0.018	No significant
2	0.290058	1.06	49	0.1	0.061	No significant
3	0.145741	1.45	67	0.1	0.053	No significant
4	0.964838	-0.04	-3	0.1	-0.001	No significant
5	0.133919	1.50	69	0.1	0.032	No significant
6	**0.015327**	**2.42**	**111**	**0.05**	**0.027**	**Significant**
7	**0.038274**	**2.07**	**95**	**0.05**	**0.039**	**Significant**
8	0.233951	1.19	55	0.1	0.023	No significant
9	**0.011980**	**2.51**	**115**	**0.05**	**0.036**	**Significant**
10	0.627737	-0.48	-23	0.1	-0.007	No significant
11	0.201105	1.28	59	0.1	0.022	No significant
12	0.964838	-0.04	-3	0.05	-0.003	No significant
Year	**0.093903**	**1.68**	**77**	**0.1**	**0.020**	**Significant**
Winter season	0.145741	1.45	67	0.1	**0.019**	No significant
Summer season	0.008169	2.64	**121**	**0.05**	**0.030**	**Significant**

Within the year, while the mean temperature in summer shows by linear regression a similar increase to its annual value (Fig 3c, R^2 = 0.3094), it shows no clear trend in winter (Fig 3b, R^2 = 0.011). In summer, this linear regression model explains about 31% of the interannual variability of SST.

The seasonal Kendall test generates an overall figure for the year that may not include monthly or seasonal statistics (Anghileri et al., 2014). Therefore, we used the annual seasonal (winter, summer) and monthly means to repeat the Mann-Kendall test and the Sen method overall years considered. In winter, the results (Table 2) show a positive MK test (S = 67), thus an increasing trend in SST over time. However, the Mann-Kendall Z parameter (1.45, Table 2) is lower than 1.65, indicating the absence of a significant trend. The P-value = 0.15, above the significant level α = 0.1, confirms the absence of a trend at the 90% confidence level.

The summer temperatures show a positive S value (139), indicating an increasing trend over time. The Mann-Kendall Z value (2.64, Table 2), more significant than 1.96, and the P-value = 0.008 below the considerable level α = 0.05 indicate the existence of a trend at the 95% confidence level. Sen's slope provides a trend of increasing SST in summer of 0.030°C/year for 1995-2020 (Table 2).

Analyses of the monthly water temperature time series at Hon Dau station show varying trends throughout the year (Fig. 2). On the linear regressions, SST seems to increase from February to September and downward in October, December, and January. In particular, the linear regressions for June, July, and September show R^2 values of 0.24, 0.22, and 0.23, respectively (Fig. 4).

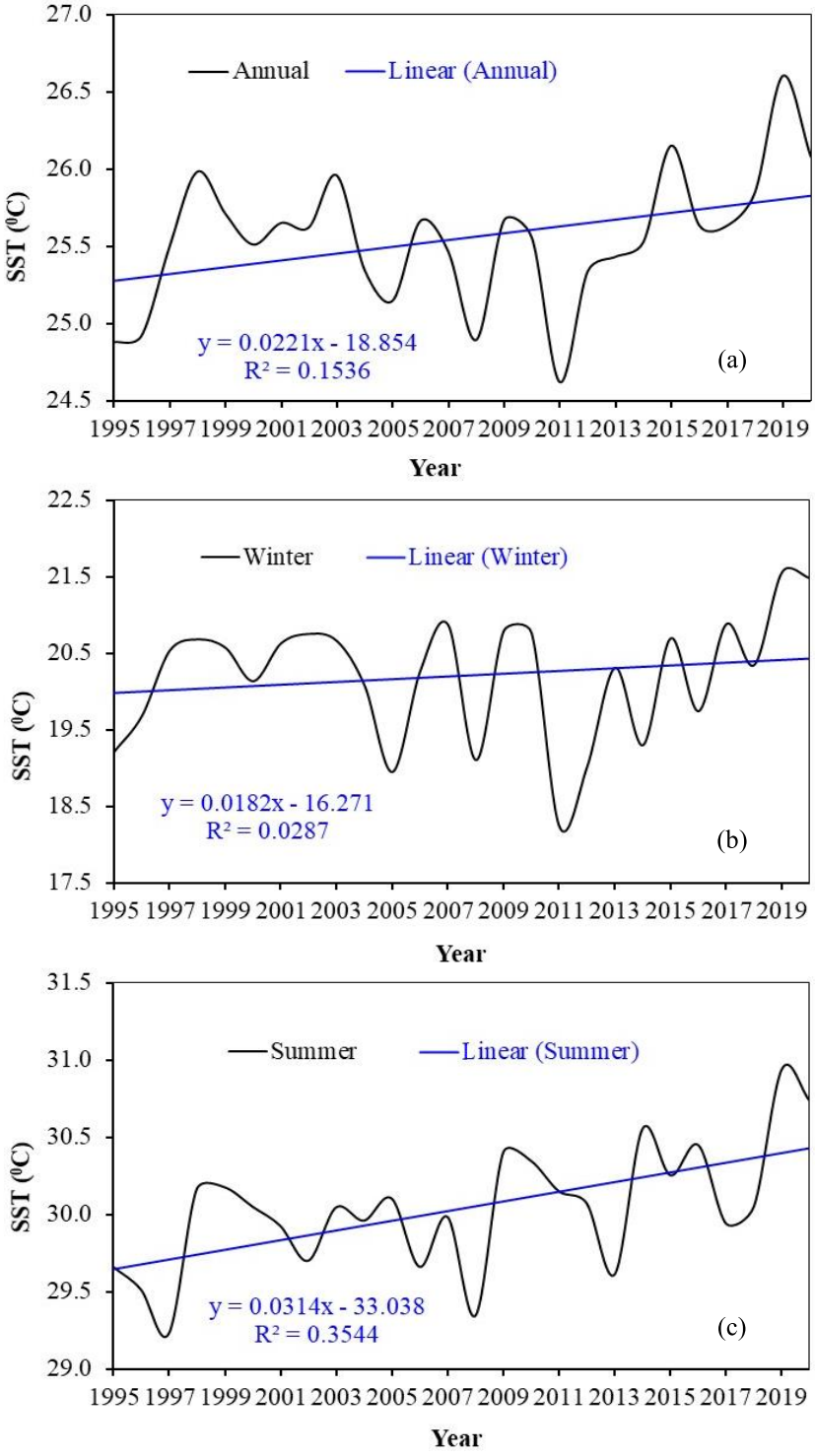

Figure 3. Annual average SST values and its trends from 1995 to 2020 at Hon Dau station: (a) over the full year, (b) in winter (December to March), and (c) in summer (June to September)

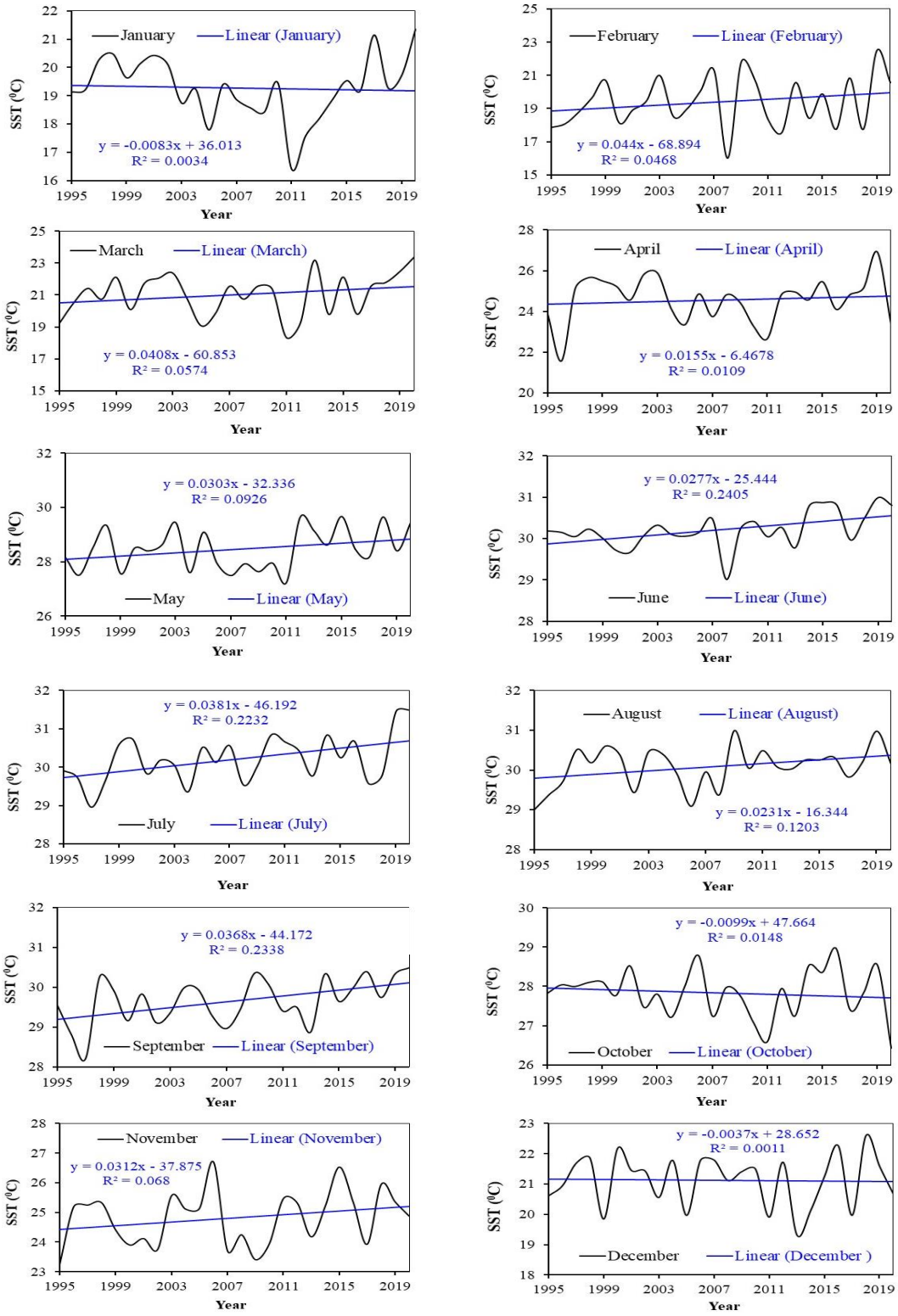

Figure 4. Trend of monthly SST from 1995 to 2020 at Hon Dau station

However, the application of the MK test indicates that there is no statistically significant trend for most months of the year. The negative S-parameter in January, April, October, and December show a downward trend of SST in these months.

A significant positive trend was also found in June, July. September with S values of 111, 95, and 155, respectively (Table 2), and P-values (0.0153 for June, 0.0383 for July, and 0.0120 for September) below the significant level $\alpha = 0.05$, which confirm the existence of a trend at a 95% confidence level. The Z parameter (2.07-2.51, Table 2), greater than 1.96, demonstrates a significant trend of increasing SST for June, July, and September. The calculation of Sen's slopes then gives increasing trends in monthly SST of 0.027°C/year in June, 0.039°C/year in July, and 0.036°C/year in September.

However, with the significant level $\alpha = 0.1$, they did not pass the MK test because the P-value is more significant than 0.1. The positive S-parameter values in February, March, May, August, and November indicate an increasing trend of SST in these months. Still, these are not significant as the P-values are greater than 0.1 (Table 2).

3.3. Trends of SST for the period 2008-2020

To access the recent trend of SST in Hon Dau, the measured data were analyzed separately by the Mann-Kendall test and Sen's slope estimator for the period 2008-2020. The result (Table 3) shows positive values of the Mann-Kendall S-parameter at all time scales (month, season, and year). This means that SST has a clear upward trend over time.

For the annual trend, the Mann-Kendall test Z-parameter (2.5, Table 3) is higher than 1.65. The P-value = 0.0124 is below the significant level $\alpha = 0.05$ (Table 3), indicating the existence of a trend with a 95% confidence level. Based on Sen's slope, the increasing trend of SST was 0.093°C/year at Hon Dau for 2008-2020 (Table 3), which is 4.65 times higher than for 1995-2020 (Table 2).

Table 3. Trend analysis of SST using Mann-Kendall test and Sen's slope for period 2008-2020

Periods/time	P-value	MK (Z)	MK Test (S)	Significance level (α)	Slope (°C/year)	Trend
1	**0.008706**	**2.62**	**44**	**0.05**	**0.237**	**Significant**
2	0.502158	0.67	12	0.1	0.069	No Significant
3	**0.044084**	**2.01**	**34**	**0.05**	**0.197**	**Significant**
4	0.246387	1.16	20	0.1	0.078	No Significant
5	0.127204	1.53	26	0.1	0.109	No Significant
6	**0.032736**	**2.14**	**36**	**0.05**	**0.080**	**Significant**
7	0.246387	1.16	20	0.1	0.066	No Significant
8	0.760332	0.31	6	0.1	0.016	No Significant
9	**0.099509**	**1.65**	**28**	**0.1**	**0.047**	**Significant**
10	0.669334	0.43	8	0.1	0.047	No Significant
11	0.246387	1.16	20	0.1	0.096	No Significant
12	0.502158	0.67	12	0.1	0.077	No Significant
Year	**0.012372**	**2.50**	**42**	**0.05**	**0.093**	**Significant**
Winter season	**0.058588**	**1.89**	**32**	**0.1**	**0.187**	**Significant**
Summer season	0.246387	1.16	20	0.1	0.057	No Significant

In the winter, the Mann-Kendall parameter Z (1.89) is more significant than 1.65, and the P-value = 0.059 is below the considerable level $\alpha = 0.1$ (Table 3). This means a significant trend in seasonal SST, with a value of 0.187°C/year. In summer, on the other hand, the P-value = 0.246 is higher than the considerable level $\alpha = 0.1$ (Table 3), which indicates that there is no trend at the 90% confidence level in this season for 2008-2020.

The MK test and Sen slope were also applied to the monthly data for 2008-2020. As

for the period 1995-2020, the results showed that there is no statistically significant trend in most of the months of the year: February, April, May, July, August, October, November, and December, as the P-values are greater than 0.1 (Table 3). The other months showed a clear trend and met the criteria for the significant level $\alpha = 0.1$ (September), and $\alpha = 0.05$ (January, March, June, and September). The slope of the increasing SST is highest in January, with 0.237°C/year, followed by that of March, June, and September, with 0.197°C/year, 0.08°C/year, and 0.047°C/year, respectively (Table 3). It should be noted that the average water temperatures in June and September showed a clear upward trend clearly over the two periods, however with slopes over 2008-2020 2.96 and 1.31 times higher than over 1995-2020 for June and September, respectively.

4. Discussions

SST varies considerably depending on the meteorological and climatic forcings in the region. In particular, SST in the East Sea, as well as in the Hai Phong coastal area, is mainly driven by the seasonal reverse monsoon winds blowing from the southwest in summer and from the northeast in winter (Vinh et al., 2018; Ku and Tseng, 2020), and the Pacific El Niño-Southern Oscillation (ENSO). For example, satellite and in situ measurements have revealed substantial warming of the East Sea during El Niño, caused by the anomalous wind that is crucial for the warming process (Wang et al., 2002; Xiao et al., 2018). Furthermore, a double peak in the SST evolution after El Niño events has been observed, with maxima occurring in February and August (Kim and An, 2021). In the Hai Phong coastal area, the annual seawater temperature time series at Hon Dau Station shows a significant interannual variation over 1995-2020 between the lowest value (24.63°C in 2011) and the highest value (26.6°C in 2019). From the ONI provided by NOAA, it can be deduced that during the period 1995-2020, there were nine El Niño events and twelve La Niña events (Table 4).

Table 4. Classification of ENSO events from 1995 to 2020

El Niño events				La Niña events		
Weak (4)	Moderate (3)	Strong (1)	Very Strong (2)	Weak (5)	Moderate (3)	Strong (4)
2004-2005	1994-1995	2009-2010	1997-1998	2000-2001	1995-1996	1998-1999
2006-2007	2002-2003		2015-2016	2005-2006	2011-2012	1999-2000
2014-2015				2008-2009	2020-2021	2007-2008
2018-2019				2016-2017		2010-2011
				2017-2018		

Among them, there were two very strong El Niño events (1997-1998: ONI maximum = 2.4; 2015-2016: ONI maximum = 2.6), one strong El Niño event (2009-2010: ONI maximum = 1.6), and four strong La Niña events (1998-1999: ONI maximum = 1.6; 1999-2000: ONI maximum = 1.7; 2007-2008: ONI maximum = 1.6; 2010-2011: ONI maximum = 1.6). ENSO conditions impacted SST in this region. The lower annual sea surface temperature in 2008 and 2011 (Fig. 3a) corresponded to intense La Niña events in 2007-2008 and 2010-2011. On the other hand, the higher annual sea surface temperature in 1998, 2015 also corresponded to extreme El Niño events (1997-1998, 2015-2016). However, the amplitude of SST and ENSO events is not entirely straightforward, and other factors are affecting SST variations. For example, in 2019, there was a weak El Niño event (ONI maximum =0.9), but the average annual SST in that year was the highest (26.6°C) from 1995 to 2020; conversely, there was a relatively high

average yearly temperature (25.51°C) in 2000 when extreme La Niña events occurred in this year. It should be noted that El Niño or La Niña in the region affects the summer monsoon, which can occur in Southeast Asia with a lag of several months compared to the phenomenon occurring in the Central Pacific. An example of ENSO's impact on the Mekong River discharge increased enormously in post-Niña years and decrease in post-Niño years (Ha et al., 2018).To examine the relationship between ENSO and SST, cross-correlation analysis was used to detect their correlations. For two time series SST(t) and ONI(t) with length n, where t=1, 2…n, the cross-correlation R(τ) at delay τ can be referred to Ding et al. (2001) and Wang et al. (2018).

$$R(\tau) = \frac{\sigma_{SSTONI}(\tau)}{\sqrt{\sigma_{SST}\sigma_{ONI}}} \quad (7)$$

Where $\sigma_{SSTONI}(\tau)$ is the lag τ cross-covariance between SST(t) and ONI (t), σ_{SST} and σ_{ONI} are the variance of SST(t) and ONI (t), respectively.

In addition, the empirical mode decomposition (EMD) method was used to identify the impact of ENSO on the SST variation (Wang et al., 2018). This method adaptively decomposes an input series into several intrinsic mode functions (IMF) having equal numbers of zero-crossing and extrema (Huang et al., 1998). Envelopes of Emin(t) and Emax(t) are estimated from interpolation between local minima and maxima, respectively (Huang et al., 2003). The EMD procedure can ascertain the dominant modes in the series SST(t) and then iteratively subtract the less dominant modes that are local mean values in the series, $(E_{min}(t)+E_{max}(t))/2$. This procedure is terminated if all the dominant modes are identified. The local mean IMF value extracted is zero.

The detailed procedure can be expressed as:

$$SST(t) = \sum_{j=1}^{M} d_j(t) + r(t) \quad (8)$$

where r(t) is a monotonic function and reflects the trend of the series SST (t). $\{d_j(t)\}_j=1^M$ denotes M IMFs within the series. To minimize problems of pseudo - IMF signal and mode confusion, the mirroring extension method that adds extrema using mirror symmetry was applied to restrain end effects (Rilling et al., 2003).

According to Wu and Huang (2014), the average period of each IMF can be calculated based on the length of original data (n) and the number of peaks:

$$P_k = \frac{n}{n_{pk}} \quad (9)$$

where P_k is the average period of IMF k^{th}, n is the length of original data, and n_{pk} is the number of local peak values of the IMF k^{th}.

The EMD method was used to evaluate the impact of ENSO on interannual sea-level variability in the Pearl River Estuary (Wang et al., 2018), coastal sea-level variability, and extreme events in Cordoba, Colombian Caribbean Sea (Genes et al., 2021). Based on the observed data at some Vietnamese coastal stations and an application of the EMD method, Huy et al. (2017a) showed that the effects of ENSO on SST tend to increase from the north to the south.

Based on the EMD method, IMF signals were identified from the time series of SST at the Hon Dau station (Fig. 5). The period of each IMF signal has been defined: IMF1 shows a period oscillation of around 6 months, IMF2 presents typical oscillations of 10.1 months, IMF3 oscillates mainly between frequencies of 24 months (2 years), IMF4 ranges from 62.4 months (5.2 years), and IMF5 ranges about 13.0 years. The periods of these signals ranged from seasonal (0.50 years), annual (0.84 years), interannual (2.0, 5.2 years), and decadal timescales (13.0 years). The periods of interannual variation, 2.0-year for IMF3 and 5.2-year for IMF4, were within the El Niño/La Niña cycle of 2-7 years. Therefore, a new IMF3.4, the sum of IMF3 and IMF4, was created to represent the signal of sea-level response to ENSO. Comparing IMF3.4 with ONI showed good agreement between the two signals (Fig. 6b).

A cross-correlation analysis was carried out between IMF3.4 and ONI delayed by 8 months. The results (Fig. 6a) indicated a high correlation between the two signals (maximum of 0.22, exceeding the 95% lower (-0.01) and upper (0.01) confidence thresholds) after an 8 month delay of the ONI. The comparison was made between the IMF3.4 mode and the ONI delayed by 8 months shows similar patterns of variability to the ENSO phenomena, presenting high values as a result of the occurrence of El Niño events (1997-1998, 2009-2010, and 2015-2016) and low values related to the occurrence of La Niña events (1995-1996, 1999-2000, 2011-2012). These results showed that IMF3 and IMF4 identified in the EMD analysis, which was around 0.6-0.9°C, represent the effect of the ENSO phenomenon on the SST at the Hon Dau station. The total influence of ENSO contributed a maximum of about 1.2°C (-0.7 to 0.5°C) on the SST in this region.

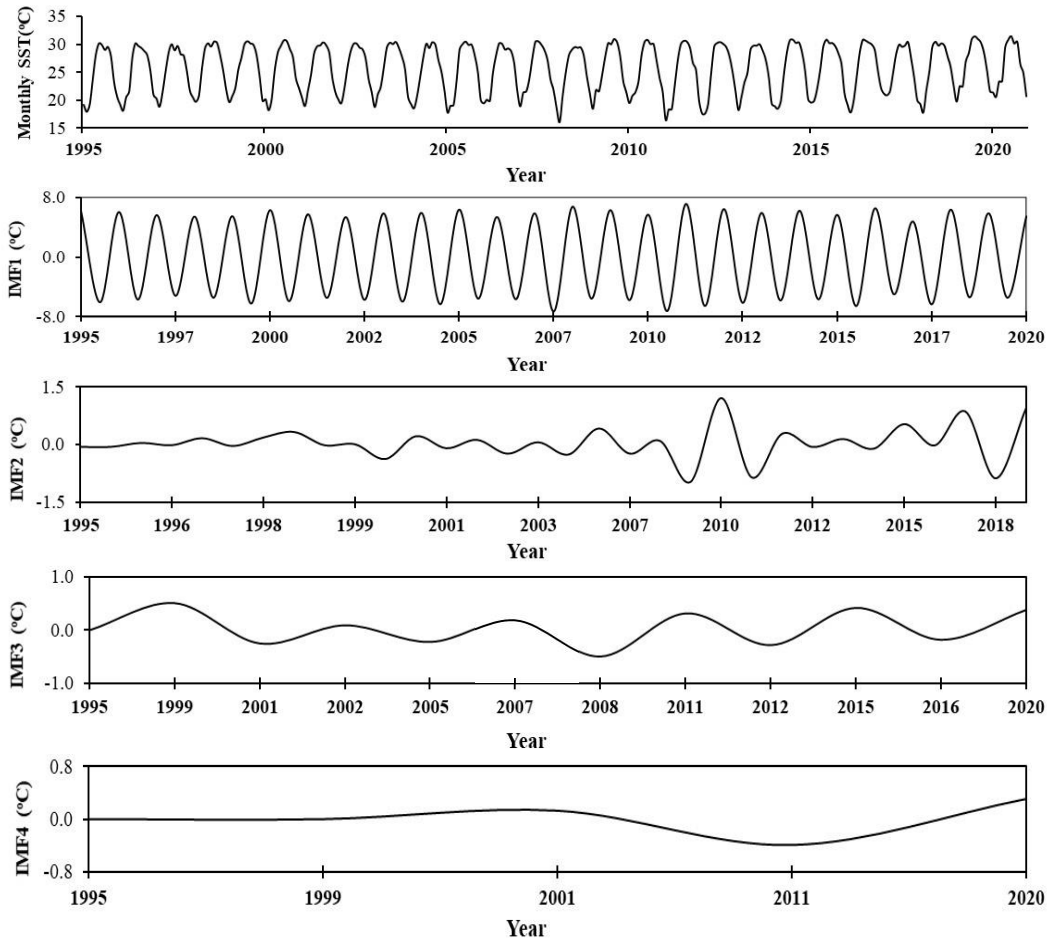

Figure 5. Monthly SST and intrinsic mode function (IMF) signals identified by EMD of SST at Hon Dau Station

According to Huy et al. (2017a), on the southern waters of the East Sea, the period of IMFs changed from the central region to the south part of the East Sea. At Son Tra (Da Nang), IMF4 (3.2 years) and IMF5 (5.3 years) were within the El Niño/La Niña cycle of

2-7 years. However, other stations (Quy Nhon, Phu Quy, Vung Tau), besides IMF4 (2.3-2.4 years) and IMF5 (3.2-4.0 years), there was a more IMF6 with period 5.9-6.5 years, also within the El Niño/La Niña cycle. The different temperature regimes can explain this difference with our results in the north and south parts of the East Sea. Every year, with one maximum and one minimum, the IMF1 signal of the SST of the North East Sea has around six months. Meanwhile, the southern East Sea SST has more than two maxima and two minima every year. Therefore, the IMF1 signal of the SST of the South East Sea has a period of around 3.0-4.2 months (Huy et al., 2017b).

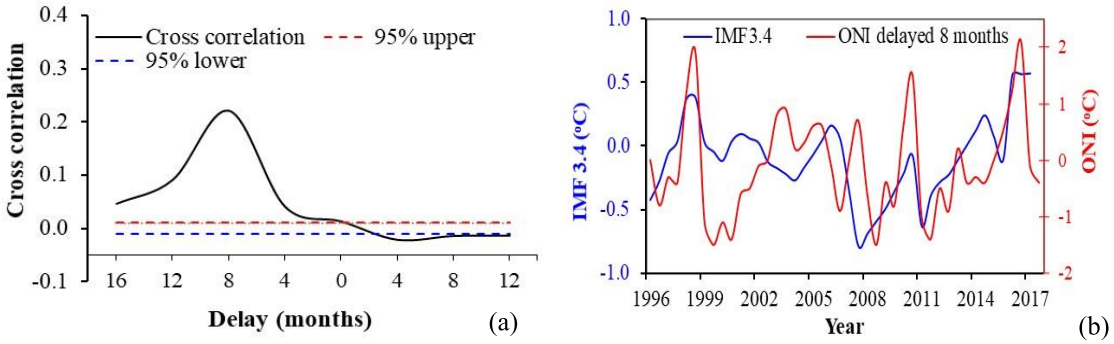

Figure 6. Relationship between SST and the ENSO phenomena. (a) Cross-correlation of IMF3.4 and ONI (b) Comparison of IMF 3.4 with ONI delayed by 8 months

Many previous studies indicated that the SST highly correlated with the ENSO phenomenon in the East Sea. Wang et al. (2002) reported an intense ES warm event in 1997-1998, closely related to the El Niño event (same as our results, see Fig. 3a), and the variability of cold winter tongue in the ES was closely correlated with the Nino3 SST. Klein et al. (1999), based on 40 years of ship observations and 10-15 years of satellite data, reported that enhanced subsidence during El Niño reduces cloud cover and increases the solar radiation absorbed by the ocean, thereby leading to improved SST in the East Sea. The correlation coefficient between the ENSO index and the SST reached 0.55 with a lag time of about 5 months from 1952 to 1992. In contrast, Fang et al. (2006) found that the first empirical orthogonal function of SST in the East Sea lagged the Niño3.4 index by about 8 months, characterized by basin-wide warming. Based on the high-resolution satellite data during 2003-2017, Yu et al. (2019) confirmed a significant correlation between the SST anomaly and the Niño3.4 index in the East Sea. The ENSO signal leads by 8 months.

In this study, the MK test showed trends for the series of SST with different statistical significance. Some months had a negative trend, but not all were statistically significant. The trend of increasing annual SST was confirmed in the results of this study, with the slope of 0.020°C/year and 0.093°C/year for the period 1995-2020 and 2008-2020, respectively. Using the MK test and Sen's slope, Ca (2017) reported that the increasing trend of SST at Hon Dau Station was 0.010 ± 0.012°C/year in 1956-2012 (with increased reliability of data over the late period). One reason for the disparity between these results is the rapid increase in water temperatures in recent years. According to NOAA (2021), the decadal surface global temperature anomaly for 2011-2020 was 0.82°C and surpassed the previous decadal (2001-2010) value of 0.62°C. Over the region, Fang et al. (2006)

reported an acceleration of SST increase in the East Sea, with rates of 0.026°C/year and 0.05°C/year over the periods 1982-2004 and 1993-2003, respectively.

It is worth noting that there are increasing trends in SST in early (June) and late (September) summer over both periods. In June, SST increased by 0.026°C/year over 1995-2020 and 0.08°C/year over 2008-2020. In September, the mean SST increased by 0.036°C/year for 1995-2020 and 0.047°C/year for 2008-2020. This suggests the possibility of a long summer with high temperatures in the region due to climate change. These are initial estimates, but they are consistent with the warnings of Wang et al. (2021) that from 1952 to 2011, the length of summer increased from 78 to 95 days and that of spring, autumn, and winter decreased from 124 to 115, 87 to 82, and 76 to 73 days, respectively. Furthermore, trends of the seasonal increase in SST were assessed in this study, but these trends exhibit a higher uncertainty than the yearly values. The significant rising trend (at the 95% confidence level) in summer SST for 1995-2020 of 0.030°C/year falls between the trend of 0.042°C/year for the East Sea basin average in 2003-2017 (Yu et al., 2019), and the trend of 0.012°C/year for the same basin in 1959-2008 (Yang and Wu, 2012). Such disparities can be explained by differences in location (space), data series periods, and calculation methods (some authors refer to trend obtained by linear regression). For winter, the SST trend is not apparent for 1995-2020 as it did not meet the condition $\alpha = 0.1$ (90% confidence level, Table 2). In contrast, over the period 2008-2020, the trend of increasing SST in winter was evident (at 90% confidence level), with a slope of 0.18°C/year. The trend seems more pronounced in summer over 1995-2020 than over 2008-2020. The above analyses highlight the uncertainty associated with the statistical analysis of trends by the Mann-Kendall test and the Sen' slope. The uncertainly can be related to seasonal increases and decreases over specific periods; the smoothing effect on increases and decreases by the trend function over the long term; cyclical rises and falls over irregular periods, and some random components (Charles, 2016; Khaliq et al., 2009). In the context of this study, ENSO events and their effects may have significantly affected the different seasonal and monthly trends of SST over both periods. More than one method should be considered for analysis of trends, as suggested by Khaliq et al. (2009), Kundzewicz and Robson (2013), and implemented by Yue et al. (2002) and Kisi (2015). According to Wang et al. (2015), using more than one approach in trend analysis allows for the interpretation of results amidst existing uncertainties.

5. Conclusions

This study examines the trends of monthly, seasonal, and annual SST at Hon Dau station (Hai Phong coastal area), using the Mann-Kendall test and the Sen's slope. It also compared significant trends over 1995-2020 and 2008-2020. The study results confirm an increasing trend in annual SST, which was 0.02°C/year over the period 1995-2020, and increased significantly to 0.093°C/year over 2008-2020. SST also increased in June and September by 0.027°C/year and 0.036°C/year, respectively, for 1995-2020, and by 0.08°C/year and 0.047°C/year, respectively, for 2008-2020.

The uncertainty is more remarkable for monthly or seasonal trends than yearly values. A seasonal movement was detected for 1995-2020, but some factors seem to impact the statistical uncertainty over 2008-2020 significantly. Interannual SST variability in the Hai Phong coastal area (at the Hon Dau station) for 1995-2020 was related to ENSO phenomena. They were signals named IMF3 and IMF4 with ~2 and ~5.2 years' cycles,

respectively. A combined signal (IMF3.5) had a maximum correlation of 0.22 with ONI delayed by 8 months. So, ENSO events took ~ 8 months to affect SST at Hai Phong coastal area for 1995-2020, causing a variation of SST within 1.2°C.

Acknowledgments

This study is benefited from the support of VAST05.05/21-22, NĐT.97.BE/20 and ĐT.MT.2017.792 projects. This paper also contributes to the LOTUS International Joint Laboratory (http://lotus.usth.edu.vn).

References

ADB, 2013. Vietnam: Environment and Climate Change Assessment. https://www.adb.org/documents/viet-nam-environment-and-climate-change-assessment.

Alemu Z.A., Dioha M.O., 2020. Climate change and trend analysis of temperature: the case of Addis Ababa, Ethiopia. Environ Syst. Res., 9, 27, https://doi.org/10.1186/s40068-020-00190-5.

Ali R., Kuriqi A., Abubaker S., Kisi O., 2019. Long-Term Trends and Seasonality Detection of the Observed Flow in Yangtze River Using Mann-Kendall and Sen's Innovative Trend Method. Water, 11(9), 1855. https://doi.org/10.3390/w11091855.

Anghileri D., Pianosi F., Soncini-Sessa R., 2014. Trend detection in seasonal data: From hydrology to water resources. J. Hydrol., 511, 171-179. https://doi.org/10.1016/j.jhydrol.2014.01.022.

Burn D.H., Hannaford J., Hodgkins G.A., Whitfield P.H., Thorne R., Marsh T., 2012. Reference hydrologic networks II. Using reference hydrologic networks to assess climate-driven changes in streamflow. Hydrol. Sci. J., 57, 1580-1593. Doi: 10.1080/02626667.2012.728705.

Ca V.T., 2017. A Climate Change Assessment via Trend Estimation of Certain Climate Parameters with In Situ Measurement at the Coasts and Islands of Vietnam. Climate, 5(2), 36. https://doi.org/10.3390/cli5020036

Chandler R.E., E.M. Scott, 2011. Statistical Methods for Trend Detection and Analysis in the Environmental Sciences. John Wiley. Chichester, U.K., 368p.

Charles O., 2016. Statistical Uncertainty in Hydrometeorological Trend Analyses. Advances in Meteorology. Article ID 8701617, 26p. https://doi.org/10.1155/2016/8701617.

Chung T.V., Long B.H., 2016. Effects of temperature field and abnormal variations of sea water level in east Vietnam sea in relationship to global climate change. Vietnam Journal of Marine Science and Technology, 16(3), 255-266. https://doi.org/10.15625/1859-3097/16/3/7533.

Davis J.C., 2002. Statistics and Data Analysis in Geology, Third Edition. John Wiley and Sons, New York.

Ding X., Zheng D., Chen Y., Zhao J., Li Z., 2001. Sea level changes in Hong Kong from tide gauge measurements of 1954-1999. J. Geodesy, 74, 683-689. https://doi.org/10.1007/s001900000128.

Dong J., Crow W.T., Duan Z.,Wei L., Lu Y., 2019. A double instrumental variable method for geophysical product error estimation. Remote Sens. Environ., 225, 217-228. Doi: 10.1016/j.rse.2019.03.003.

Duan Z., et al., 2019. Hydrological evaluation of open-access precipitation and air temperature datasets using SWAT in a poorly gauged basin in Ethiopia. J. Hydrol., 569, 612-626. Doi: 10.1016/j.jhydrol.2018.12.026.

Duy Vinh V., Ouillon S., Van Uu D., 2018 Estuarine Turbidity Maxima and Variations of Aggregate Parameters in the Cam-Nam Trieu Estuary, North Vietnam, in Early Wet Season. Water, 10, 68. http://dx.doi.org/10.3390/w10010068.

EPA, 2012. 5.3 Temperature. In Water: Monitoring and Assessment. Retrieved from http://water.epa.gov/type/rsl/monitoring/vms53.cfm.

Gao H., Birkel C., Hrachowitz M., Tetzlaff D., Soulsby C., Savenije H.H.G., 2019. A simple topography-driven and calibration-free runoff generation module. Hydrol. Earth Syst. Sci., 23, 787-809. Doi: 10.5194/hess-23-787-2019.

Genes L.S., Montoya R.D., Osorio A.F., 2021. Costal sea level variability and extreme events in Mo˜nitos, Cordoba, Colombian Caribbean Sea. Continental Shelf Research, 228, 104489. https://doi.org/10.1016/j.csr.2021.104489.

Groves C.R., Game E.T., Anderson M.G., Cross M., Enquist C., Ferdaña Z., Girvetz E., Gondor A., Hall K.R., Higgins J., Marshall R., Popper K., Schill S.,

Shafer S.L., 2012. Incorporating climate change into systematic conservation planning. Biodivers. Conserv., 21, 1651-1671. https://doi.org/10.1007/s10531-012-0269-3.

Güçlü Y.S., 2018. Multiple Şen-innovative trend analyses and partial Mann-Kendall test. Journal of Hydrology, 566, 685-704. https://doi.org/10.1016/j.jhydrol.2018.09.034.

Ha D.T., Ouillon S., Vinh G.V., 2018. Water and suspended sediment budgets in the lower Mekong from high-frequency measurements (2009-2016). Water, 10, 846. Doi:10.3390/w10070846.

Hirsch R.M., Slack J.R., Smith R.A., 1982. Techniques of trend analysis for monthly water quality data. Water Resour. Res., 18, 107-121. Doi: 10.1029/WR018i001p00107.

Hirsch R.M., Slack J.R., 1984. A nonparametric trend test for seasonal data with serial dependence. Water Resour. Res., 20, 727-732. Doi: 10.1029/WR020i006p00727.

Huang N.E., Shen Z., Long S.R., Wu M.C., Shih H.H., Zheng Q., Yen N.C., Tung C.C., Liu H.H., 1998. The empirical mode decomposition and the Hilbert spectrum for nonlinear and non-stationary time series analysis, Proc. Roy. Soc. London A, 454, 903-995.

Huang N.E., Wu M.L., Qu W., Long S.R., Shen S.S.P., Zhang J.E., 2003. Applications of Hilbert-Huang transform to non-stationary financial time series analysis. Appl. Stoch. Model. Bus., 19, 245-268. https://doi.org/10.1002/asmb.501.

Huy L.Q., Thuc T., Hien N.X., Uu D.V, 2017a. Effects of ENSO on the intraseasonal oscillations of sea surface temperature and wind speed along Vietnam's coastal areas. Vietnam Journal of Science, Technology and Engineering, 59(3), 85-90. https://doi.org/10.31276/VJSTE.59(3).85

Huy L.Q., Hien N.X., Thuc T., Dat P.T., 2017b. Analysis of the variation in sea surface temperatures and the influence of ENSO in the coastal region of the south central of Viet Nam. Journal of Climate Change Science, Vol 1, 67-74 (in Vietnamese).

Kendall M.G., 1975. Rank correlation methods. 4th Edition, Charles Griffin, London.

Khaliq M.N., Ouarda T. B. M. J., Gachon P., Susham L. A., St-Hilaire A, 2009. Identification of hydrological trends in the presence of serial and cross correlations: A review of selected methods and their application to annual flow regimes of Canadian rivers. Journal of Hydrology, 368(1-4), 117-130. https://doi.org/10.1016/j.jhydrol.2009.01.035.

Kim S., An S., 2021. Seasonal Gap Theory for ENSO Phase Locking, Journal of Climate, 34(14), 5621-5634. https://doi.org/10.1175/JCLI-D-20-0495.1.

Kisi O., 2015. An innovative method for trend analysis of monthly pan evaporations. J. Hydrol., 527, 1123-1129. https://doi.org/10.1016/j.jhydrol.2015.06.009.

Klein S.A., Soden B.J., Lau N.C., 1999. Remote sea surface temperature variations during ENSO: Evidence for a tropical atmospheric bridge. Journal of Climate, 12(4), 917-932. https://doi.org/10.1175/1520-0442(1999)012<0917:RSSTVD>2.0.CO;2.

Kundzewicz Z.W., Robson A.J., 2004. Change detection in hydrological records a review of the methodology. Hydrological Sciences Journal, 49(1), 7-20. https://doi.org/10.1623/hysj.49.1.7.53993.

Lefebvre J.P., Ouillon S., Vinh V.D., Arfi R., Panche J.Y., Mari X., Van Thuoc C., Torréton J.P., 2012. Seasonal variability of cohesive sediment aggregation in the Bach Dang-Cam Estuary, Haiphong (Vietnam). Geo-Mar. Lett., 32, 103-121. http://dx.doi.org/10.1007/s00367-011-0273-8.

Minh N.N., Marchesiello P., Lyard F., Ouillon S., Cambon G., Allain D., Van Uu D., 2014. Tidal characteristics of the Gulf of Tonkin. Cont. Shelf Res., 91, 37-56. https://doi.org/10.1016/j.csr.2014.08.003.

MONRE, 2016. Climate change and sea level rise scenarios for Viet Nam. Hanoi.

NOAA National Centers for Environmental Information, 2021. State of the Climate: Global Climate Report for Annual 2020, published online January 2021, retrieved on October 7, 2021 from https://www.ncdc.noaa.gov/sotc/global/202013.

NOAA, 2020. https://origin.cpc.ncep.noaa.gov/products/analysis_monitoring/ensostuff/ONI_v5.php. Access on December 31, 2020.

O'Connor M.I., Bruno J.F., Gaines S.D., Halpern B.S., Lester S.E., Kinlan B.P., Weiss J.M., 2007. Temperature control of larval dispersal and the implications for marine ecology, evolution, and conservation. Proc Natl Acad Sci U S A. 2007 Jan 23, 104(4):1266-71. Doi: 10.1073/pnas.0603422104. Epub 2007 Jan 9. PMID: 17213327; PMCID: PMC1764863.

Ozgenc Aksoy A., 2017. Investigation of sea level trends and the effect of the north atlantic oscillation (NAO) on the black sea and the eastern mediterranean sea. Theor Appl Climatol, 129, 129-137. https://doi.org/10.1007/s00704-016-1759-0.

Pasquero C., 2008. Water masses: Conservation of heat and salt. Upper, intermediate waters. In ESS 130: Physical Oceanography. Retrieved from http://www.ess.uci.edu/~cpasquer/classes/ess130/notes/lec18.pdf.

Pohlert T., 2020. Non-Parametric Trend Tests and Change-Point Detection [R package trend version 1.1.4]. https://cran.r-project.org/web/packages/trend/vignettes/trend.pdf.

Rilling, G., Flandrin, P., Goncalves, P., 2003. On Empirical Mode Decomposition and Its Algorithms. IEEE-EURASIP Workshop on Nonlinear Signal Image Process. NSIP-03. Grado Italy.

Sang Y.-F., Wang Z., Liu C., 2014. Comparison of the MK test and EMD method for trend identification in hydrological time series. J. Hydrol., 510, 293-298. Doi: 10.1016/j.jhydrol.2013.12.039.

Scholes I.J., et al., 2014. Terrestrial and inland water systems, in Climate Change 2014: Impacts, Adaptation, and Vulnerability, Part A: Global and Sectoral Aspects, Contribution of Working Group II to the 5th Assessment Report of the IPCC, Cambridge University Press, NY, 271-359.

Sen P.K., 1968. Estimates of the Regression Coefficient Based on Kendall's Tau. Journal of the American Statistical Association, 63(324), 1379. https://doi.org/10.2307/2285891.

Şen Z., 2012. Innovative trend analysis methodology. J. Hydrol. Eng., 17, 1042-1046. Doi: 10.1061/(ASCE)HE.1943-5584.0000556.

Thanh T.D., San B.Q., Can N.V., Lan T.D., Quan N.V., Dieu L.V., Thu N.T., Tu T.A., Anh N.T.K, 2015. Nature and environment in Haiphong coastal zone. ISBN: 978-604-913-396-1. Published by Publishing House for Science and Technology. Vietnam Academy of Science and Technology (VAST) (in Vietnamese).

Tosunoglu F., Kisi O., 2017. Trend Analysis of Maximum Hydrologic Drought Variables Using Mann-Kendall and Şen's Innovative Trend Method. River Res. Appl., 33, 597-610. https://doi.org/10.1002/rra.3106.

Vinh V.D., Uu D.V., 2013. The influence of wind and oceanographic factors on characteristics of suspended sediment transport in Bach Dang estuary. J. Mar. Sci. Technol., 3, 216-226.

Vinh V.D., Ouillon S., Thanh T.D., Chu L.V., 2014. Impact of the Hoa Binh dam (Vietnam) on water and sediment budgets in the Red River basin and delta. Hydrol. Earth Syst. Sci., 18, 3987-4005. https://doi.org/10.5194/hess-18-3987-2014.

Vinh V.D , Thanh T.D., 2014. Characteristics of current variation in coastal area of red river delta - results of research applied the 3D numerical model. Journal of Marine Science and Technology, 14(2), 139-148.

Vinh V.D., Ouillon S., 2021. The double structure of the Estuarine Turbidity Maximum in the Cam-Nam Trieu mesotidal tropical estuary, Vietnam, Marine Geology, 442, 106670. Doi: 10.1016/j.margeo.2021.106670.

Wahl T., J. Jensen, Frank T., Haigh I.D., 2011. Improved estimates of mean sea level changes in the German Bight over the last 166 years, Ocean Dyn., 61, 701-715. Doi: 10.1007/s10236-011-0383-x.

Wang W., Chen Y., Becker S., Liu B., 2015. Variance correction prewhitening method for trend detection in autocorrelated data. Journal of Hydrologic Engineering, 20(12), 04015033. Doi: 10.1061/(ASCE)HE.1943-5584.0001234.

Wang J., et al., 2021. Changing lengths of the four seasons by global warming. Geophysical Research Letters, 48, e2020GL091753. https://doi. org/10.1029/2020GL091753.

Wang L., Li Q., Mao X.Z., Bi H., Yin P., 2018. Interannual Sea level variability in the pearl river

Estuary and its response to El Ni˜no-southern oscillation. Global Planet. Change, 162, 163-174. Doi: 10.1016/j.gloplacha.2018.01.007.

Watson J.E., Rao M., Ai-Li K., Yan X., 2012. Climate change adaptation planning for biodiversity conservation: A review. Adv. Clim. Change Res., 3, 1-11. Available at: https://www.scipedia.com/public/Watson_et_al_2015a.

Wetzel R.G., 2001. Limnology: Lake and River Ecosystems (3rd ed.). San Diego, CA: Academic Press.

Wu Z., Huang N.E., 2004. A study of the characteristics of white noise using the empirical mode decomposition method. Proceedings of the Royal Society of London. Series A: Mathematical, Physical and Engineering Sciences, 460, 1597-1611.

Yue S., P. Pilon, G. Cavadias., 2002. Power of the Mann-Kendall and Spearman's rho tests for detecting monotonic trends in hydrological series. Journal of Hydrology, 259(1-4), 254-271. https://doi.org/10.1016/S0022-1694(01)00594-7.

Zakwan M., Ahmad Z., 2021. Trend analysis of hydrological parameters of Ganga River. Arab J. Geosci., 14, 163. https://doi.org/10.1007/s12517-021-06453-4.